SNAP: Fabrication of long coupled microresonator chains with sub-angstrom precision

M. Sumetsky* and Y. Dulashko

OFS Laboratories, 19 Schoolhouse Road, Somerset, New Jersey 08873, USA
sumetski@ofsoptics.com

Abstract: Based on the recently-introduced Surface Nanoscale Axial Photonics (SNAP) platform, we demonstrate a chain of 30 coupled SNAP microresonators spaced by 50 micron along an optical fiber, which is fabricated with the precision of 0.7 angstrom and a standard deviation of 0.12 angstrom in effective microresonator radius. To the best of our knowledge, this result surpasses those achieved in other super-low-loss photonic technologies developed to date by two orders of magnitude. The chain exhibits bandgaps in both the discrete and continuous spectrum in excellent agreement with theory. The developed method enables robust fabrication of SNAP devices with sub-angstrom precision.

OCIS codes: (060.2340) Fiber optics components; (140.3945) Microcavities; (230.3990) Micro-optical devices.

References and links

1. F. N. Xia, L. Sekaric, and Y. Vlasov, "Ultracompact optical buffers on a silicon chip," Nat. Photonics **1**(1), 65–71 (2007).
2. M. Notomi, E. Kuramochi, and T. Tanabe, "Large-scale arrays of ultrahigh-Q coupled nanocavities," Nat. Photonics **2**(12), 741–747 (2008).
3. W. Bogaerts, S. K. Selvaraja, P. Dumon, J. Brouckaert, K. De Vos, D. Van Thourhout, and R. Baets, "Silicon-on-insulator spectral filters fabricated with CMOS technology," IEEE J. Sel. Top. Quantum Electron. **16**(1), 33–44 (2010).
4. A. Melloni, A. Canciamilla, C. Ferrari, F. Morichetti, L. O'Faolain, T. F. Krauss, R. De La Rue, A. Samarelli, and M. Sorel, "Tunable delay lines in silicon photonics: coupled resonators and photonic crystals, a comparison," IEEE Photon. J. **2**(2), 181–194 (2010).
5. M. L. Cooper, G. Gupta, M. A. Schneider, W. M. J. Green, S. Assefa, F. Xia, Y. A. Vlasov, and S. Mookherjea, "Statistics of light transport in 235-ring silicon coupled-resonator optical waveguides," Opt. Express **18**(25), 26505–26516 (2010).
6. A. Canciamilla, F. Morichetti, S. Grillanda, P. Velha, M. Sorel, V. Singh, A. Agarwal, L. C. Kimerling, and A. Melloni, "Photo-induced trimming of chalcogenide-assisted silicon waveguides," Opt. Express **20**(14), 15807–15817 (2012).
7. S. Prorok, A. Yu. Petrov, M. Eich, J. Luo, and A. K.-Y. Jen, "Trimming of high-Q-factor silicon ring resonators by electron beam bleaching," Opt. Lett. **37**(15), 3114–3116 (2012).
8. M. Sumetsky, "Localization of light in an optical fiber with nanoscale radius variation," in CLEO/Europe and EQEC 2011 Conference Digest, postdeadline paper PDA_8.
9. M. Sumetsky and J. M. Fini, "Surface nanoscale axial photonics," Opt. Express **19**(27), 26470–26485 (2011).
10. M. Sumetsky, D. J. DiGiovanni, Y. Dulashko, J. M. Fini, X. Liu, E. M. Monberg, and T. F. Taunay, "Surface nanoscale axial photonics: robust fabrication of high-quality-factor microresonators," Opt. Lett. **36**(24), 4824–4826 (2011).
11. M. Sumetsky, K. Abedin, D. J. DiGiovanni, Y. Dulashko, J. M. Fini, and E. M. Monberg, "Coupled high Q-factor surface nanoscale axial photonics (SNAP) microresonators," Opt. Lett. **37**(6), 990–992 (2012).
12. M. Sumetsky, D. J. DiGiovanni, Y. Dulashko, X. Liu, E. M. Monberg, and T. F. Taunay, "Photo-induced SNAP: fabrication, trimming, and tuning of microresonator chains," Opt. Express **20**(10), 10684–10691 (2012).
13. M. Sumetsky, "Theory of SNAP devices: basic equations and comparison with the experiment," Opt. Express **20**(20), 22537–22554 (2012).
14. A. B. Matsko and V. S. Ilchenko, "Optical resonators with whispering-gallery modes—part I: Basics," IEEE J. Sel. Top. Quantum Electron. **12**(1), 3–14 (2006).
15. M. Sumetsky, P. I. Reyes, P. S. Westbrook, N. M. Litchinitser, B. J. Eggleton, Y. Li, R. Deshmukh, and C. Soccolich, "Group-delay ripple correction in chirped fiber Bragg gratings," Opt. Lett. **28**(10), 777–779 (2003).

#178745 - $15.00 USD Received 25 Oct 2012; revised 17 Nov 2012; accepted 20 Nov 2012; published 29 Nov 2012

16. F. Luan, E. Magi, T. Gong, I. Kabakova, and B. J. Eggleton, "Photoinduced whispering gallery mode microcavity resonator in a chalcogenide microfiber," Opt. Lett. **36**(24), 4761–4763 (2011).
17. A. D. Yablon, M. F. Yan, P. Wisk, F. V. DiMarcello, J. W. Fleming, W. A. Reed, E. M. Monberg, D. J. DiGiovanni, J. Jasapara, and M. E. Lines, "Refractive index perturbations in optical fibers resulting from frozen-in viscoelasticity," Appl. Phys. Lett. **84**(1), 19–21 (2004).
18. T. A. Birks, J. C. Knight, and T. E. Dimmick, "High-resolution measurement of the fiber diameter variations using whispering gallery modes and no optical alignment," IEEE Photon. Technol. Lett. **12**(2), 182–183 (2000).
19. M. Sumetsky and Y. Dulashko, "Radius variation of optical fibers with angstrom accuracy," Opt. Lett. **35**(23), 4006–4008 (2010).

1. Introduction

A remarkable fabrication precision (several nm) and low propagation loss (typically, in excess of 0.1 dB/cm, limited by the surface roughness) of miniature photonic integrated circuits have been demonstrated with modern fabrication technologies [1–4]. Despite the notable progress, the achieved high precision and low loss are still insufficient for the fabrication of long chains of coupled microresonators and other photonic structures proposed to date for efficient slowing and manipulation of light. In fact, the remaining nanoscale-small randomness of the microresonator dimensions and interface roughness lead to significant attenuation of light and collapse of the transmission band of long coupled microresonator chains [1,5]. In addition, methods developed for the reduction of fabrication errors by trimming exhibit temporal instability [6] and/or attenuation of light [7] unacceptable for super-low-loss photonic circuits.

Recently, we introduced a technological platform enabling fabrication of microphotonic circuits at the atomically-smooth surface of a drawn optical fiber with unprecedented angstrom accuracy [8–13]. This technology allowed us to fabricate a series of ultra-low-loss coupled whispering gallery mode (WGM) microresonators along the optical fiber by nanoscale variation of its effective radius (which includes both the variation of the physical fiber radius and of its refractive index). Similar to the other types of silica microresonators fabricated by melting (spherical, toroidal, bottle, etc [14].), the Q-factor of these microresonators can exceed a billion. The surface nature of WGMs [14], their slow axial propagation described by a one-dimensional Schrödinger equation [8,9,13], as well as the simplicity and accuracy of the nanoscale variation of the fiber radius [10–13] motivated us to coin the name Surface Nanoscale Axial Photonics and its abbreviation "SNAP" for this technology.

We have demonstrated the fabrication of SNAP microresonators with angstrom-scale precision by focused CO_2 laser annealing of silica fibers [10,11,13] and also by the UV radiation exposure of photosensitive Ge-doped optical fibers through an amplitude mask [10,12]. However, the chains of angstrom-precise coupled SNAP microresonators fabricated so far contained a relatively small number of microresonators due to fabrication errors growing with the length of the SNAP device. While a few angstrom precision in fabrication of multiple coupled microresonator chains is typical, a sub-angstrom precision [13] was achieved after multiple tries only. This was particularly caused by the original nonuniformity of the fiber radius, surface contamination, imperfect system alignment, and fluctuations of the beam power control system. Evidently, the future success of SNAP depends on the solution of the problem of fabrication errors.

In this paper, we demonstrate the fabrication of a SNAP device with multiple laser shots and consistently reduce the fabrication errors by iterations. We explore a CO_2 laser annealing method applicable to general types of optical fibers. A similar iterative approach for photosensitive fibers, where the effective fiber radius is treated with UV and visible light, could also be feasible [12,15,16]. The developed method allowed us to achieve a 0.7 Å precision and 0.12 Å standard deviation in the effective heights of 30 coupled microresonators. It is suggested that the demonstrated precision and standard deviation can be improved for chains of microresonators and other SNAP devices having similar and larger axial lengths.

#178745 - $15.00 USD Received 25 Oct 2012; revised 17 Nov 2012; accepted 20 Nov 2012; published 29 Nov 2012

2. Experimental setup

Our experimental setup is illustrated in Fig. 1. It consists of the SNAP fiber (SF) exposure section (Fig. 1(a)) and the fiber characterization section (Fig. 1(b)). The nanoscale effective radius variation (ERV) of the optical fiber is introduced with a CO_2 laser beam focused onto the fiber by the parabolic lens (Fig. 1(a)). The input beam power is controlled by a laser power controller and a shutter with a 1 ms switching time. Annealing the optical fiber relaxes the tension, which is frozen-in during fiber drawing [17] and causes the nanoscale ERV [10]. After the exposure, the SF is characterized at the measurement section of our setup with the microfiber scanning method (Fig. 1(b)) [18,19]. In this method, the microfiber is scanned along the SF touching it at contact points where the spectra of the microfiber coupled to the SF are measured. The spacing between the contact points (set to 10 μm) determines the axial resolution of measurements. At each contact point we measure the resonant transmission amplitude spectrum with 1.3 pm resolution using the Luna Optical Vector Analyzer. The characterization step, including measurement, saving data, and translation of the microfiber, takes 20 s. The spectra are used for the evaluation of SF performance and its ERV.

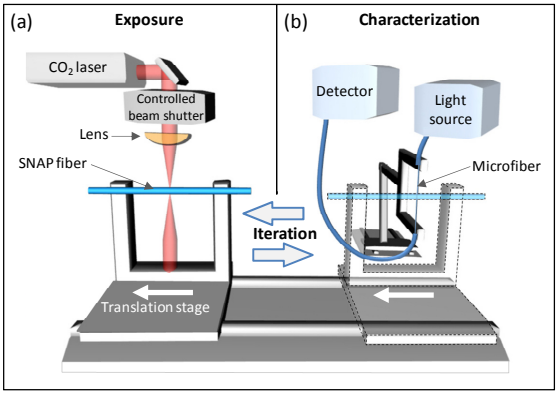

Fig. 1. Illustration of the setup for iterative fabrication of SNAP devices. (a) – Exposure section; (b) – characterization section.

3. Fabrication and correction of the microresonator chain

In our experiment, a chain of 30 strongly coupled microresonators is created along a 19 μm radius fiber. Each microresonator is introduced by a sequence of 20 CO_2 laser 0.1s/0.1s on/off exposures using the beam shutter. The spacing between microresonators is set to 50 μm. The SF is characterized by the microfiber scanning method. Figure 2(a) shows the surface plot of the resonant microfiber/SF transmission amplitude spectra. The spectra exhibit the fundamental transmission band near the wavelength $\lambda = 1564.3\,\text{nm}$ followed by a bandgap. The wavelength variation of resonances, $\Delta\lambda$ (left vertical axis), is related to the characteristic ERV, Δr_{eff} (right vertical axis), by a simple scaling relation, $\Delta\lambda/\lambda_{res} = \Delta r_{eff}/r_0$ [8,9,18], where λ_{res} = 1.56 μm is the resonance wavelength and r_0 = 19 μm is the SF radius. The full characterization time of the SF along the 1.9 mm length was 1 hour. During this time, the temperature was maintained constant within ΔT = 0.1°C. The ERV due to this temperature change was less than $\delta r = r_0(n^{-1}dn/dT + dl/l)\Delta T = 0.16$Å, where for silica we set the refractive index n = 1.46, $dn/dT = 1.2\cdot10^{-5}$/°C, and the coefficient of expansion $dl/l = 0.5\cdot10^{-6}$. To evaluate the radial nonuniformity of the microresonator chain, we determine the positions of blue-color apexes (BCAs) corresponding to each of the microresonators in Fig. 2(a). The method is justified by the theoretical calculations below. The coordinates of these apexes are plotted in Fig. 3(a). From Fig. 3(a), the radial nonuniformity of the microresonator chain in Fig. 2(a) is equal to $\delta r_{eff}^{(0)} = 6$ Å.

#178745 - $15.00 USD Received 25 Oct 2012; revised 17 Nov 2012; accepted 20 Nov 2012; published 29 Nov 2012

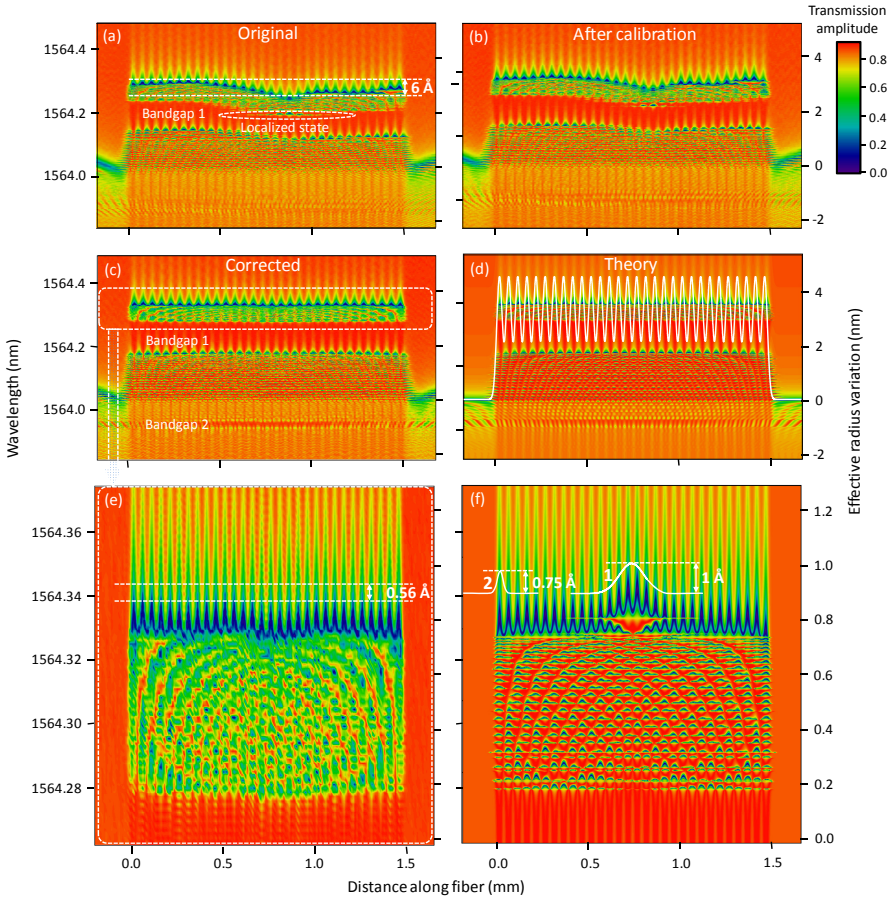

Fig. 2. Experimental characterization and theoretical modeling of the resonant transmission amplitude of the fabricated 30 coupled microresonator chain. The surface plots of experimental data are obtained with 1.3 pm resolution in wavelength and 10 μm resolution along the fiber axis. (a) – The spectral surface plot of the originally fabricated microresonator chain. (b) – The spectral surface plot of this chain after calibration exposure. (c) – The spectral surface plot of the corrected chain. (d) – The spectral surface plot of the corrected chain obtained theoretically. White solid curve is the calculated ERV. (e) – The spectral surface plot of the transmission band magnified from Fig. 2(c). (f) – Theoretical modeling of the effect of effective radius perturbations.

To improve the uniformity of the microresonator chain, we perform its correction. We start with the calibration of the laser shots. To this end, using the beam shutter (Fig. 1(a)), the m^{th} microresonator of the chain (except for the last one) is exposed to m 54 ms long shots (the length of shots is determined experimentally to arrive at the resultant local ERV of less than 0.1 Å). The spectral plot of the so-modified SF is shown in Fig. 2(b). To evaluate the change, curve 1 and 2 in Fig. 3 show the positions of BCAs corresponding to the microresonators in Fig. 2(a) and Fig. 2(b), respectively. The calculated resonance shifts (curve 3) are approximately proportional to the number of shorts, which allows us to find the average shift in the effective radius per shot as 0.07 Å. Next, we alter the radii of microresonators in order to make them equal by exposing the microresonators to the appropriate numbers of shots. The resultant spectral plot of remarkably uniform microresonator chain achieved after two iterations is shown in Fig. 2(c).

#178745 - $15.00 USD Received 25 Oct 2012; revised 17 Nov 2012; accepted 20 Nov 2012; published 29 Nov 2012

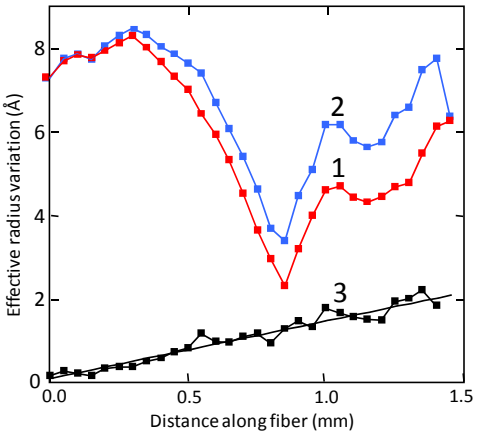

Fig. 3. The plot of BCA vertical coordinates characterizing the nonuniformity of the microresonator chain. Curve 1 and 2 shows the positions of BCAs corresponding to the microresonators in Fig. 2(a) and Fig. 2(b), respectively. Curve 3 is the difference between curves 1 and 2, which is used for calibration of the shots.

4. Theoretical analysis

The introduced ERV of the microresonator chain can be determined by fitting the spectral surface plot in Fig. 2(c) to the analytical model, which, for the uniform chain, is taken in the form:

$$\Delta r_{eff}(z) = \Delta r_0 \begin{cases} \exp\left(-\frac{z^2}{\zeta^2}\right), & z < 0, \\ \frac{a^2}{2\pi^2\zeta^2}\left(\cos\left(\frac{2\pi z}{a}\right)-1\right)+1, & 0 < z < (N-1)a, \\ \exp\left[-\frac{(z-(N-1)a)^2}{\zeta^2}\right], & z > (N-1)a. \end{cases} \quad (1)$$

In this equation, $a = 50$ μm is the chain period, and other parameters of ERV are determined by the theory [13]. Specifically, we fit the bandgap and fundamental transmission band dimensions in Fig. 2(c) to those of the spectrum of the Schrödinger equation with the potential defined by the ERV $\Delta r_{eff}(z)$ of Eq. (1) [8,9,13],

$$\Psi_{zz} + (E(\lambda) - V(z))\Psi = 0, \qquad E(\lambda) = \kappa\Delta\lambda / \lambda_{res}, \qquad V(z) = \kappa\Delta r_{eff}(z) / r_0, \qquad \kappa = -8(\pi n / \lambda_{res})^2, \quad (2)$$

and arrive at $\Delta r_0 = 4.5$ nm and $\zeta = 15.4$ μm, the parameters of ERV shown in Fig. 2(d) (white curve). The height and modulation amplitude of the introduced ERV are $\Delta r_0 = 4.5$ nm and $\Delta r_0 a^2 / (2\pi^2\zeta^2) = 1.2$ nm, respectively. We found the remarkably good correspondence of positions of individual resonances below bandgap 1, while the actual fine spectrum of the fundamental transmission band above bandgap 1 was not well-resolved with the resolution of our measurements (1.3 pm in wavelength corresponding to 0.15 Å in ERV). The theoretical spectral plot shown in Fig. 2(d) is determined using the expression for the transmission amplitude [13],

$$T(\lambda, z) = T_0 - \frac{i\,|C|^2\, G(\lambda, z, z)}{1 + DG(\lambda, z, z)}, \quad (3)$$

#178745 - $15.00 USD Received 25 Oct 2012; revised 17 Nov 2012; accepted 20 Nov 2012; published 29 Nov 2012

where $G(\lambda, z_1, z_2)$ is the Green's function of Eq. (2) and parameters are determined by fitting the experimental data in Fig. 2(c): $T_0 = 0.85 - 0.25i$, $|C|^2 = 0.02\ \mu\text{m}^{-1}$, and $D = 0.015 + 0.02i\ \mu\text{m}^{-1}$.

Similar to the original microresonator chain shown in Fig. 2(a), the nonuniformity of the corrected chain is estimated from the variation of the vertical coordinates of BCAs at the fundamental transmission band in Fig. 2(c), which is magnified in Fig. 2(e). From Fig. 2(e), due to the smooth spatial and wavelength spectral behavior in the regions of BCAs and interpolation incorporated into the plots of the experimental data, we are able to determine BCA positions with an accuracy of ~0.01 Å. Consequently, the variation of BCA coordinates of the fabricated microresonator chain is estimated at 0.56 Å and their standard deviation at 0.12 Å. The precision of our measurements is estimated from the nonuniformity (deviation from the horizontal direction) of the discrete spectral lines situated below bandgap 1 in Fig. 2(c) and found to be close to the measurement resolution 0.15 Å. Generally, the nonuniformity of these lines determines the spectral shift due to the measurement errors and temperature variation, which can be calibrated out. The summarized fabrication precision of the microresonator chain is estimated at 0.7 Å.

Our approach for the evaluation of microresonator nonuniformity is validated by sample calculations shown in Fig. 2(f), which illustrates the effects of perturbation of the ERV of the uniform microresonator chain defined by Eq. (1) (white curve in Fig. 2(d)). In the first example, we perturb the center of this ERV by an angstrom-high and relatively wide Gaussian bump $\Delta r_1 \exp(-z^2/\zeta_1^2)$ with $\Delta r_1 = 1$ Å and $\zeta_1 = 100$ μm (white curve 1 in Fig. 2(f)). Comparison of this bump with the corresponding spectral plot of the fundamental transmission band in Fig. 2(f) confirms that wide (adiabatic) ERV perturbation envelopes the introduced shifts of BCAs. For narrower bumps, the effect of the apex shift is smaller. In the second example, we numerically correct the height of the BCA corresponding to the first microresonator of the chain, which, for the uniform chain, is shorter than others by 0.53 Å. This is accomplished using the Gaussian bump $\Delta r_2 \exp(-z^2/\zeta_2^2)$ with $\Delta r_2 = 0.75$ Å and $\zeta_2 = 25$ μm applied to the center of the first microresonator of the chain (white curve 2). This perturbation makes the height of the first BCA close to those in the middle of the chain.

5. Summary

In summary, a chain of 30 coupled SNAP microresonators is fabricated along the optical fiber with sub-angstrom precision of 0.7 angstrom and a standard deviation of 0.12 angstrom in excellent agreement with theoretical calculations. To the best of our knowledge, this result surpasses those achieved in other super-low-loss photonic technologies developed to date by two orders of magnitude. The fabrication is accomplished by application of iterative sequences of CO_2 laser shots, where each shot introduces a small ~0.1 Å change in the local fiber radius. Generally, laser shots of appropriate durations and powers can be used for the nanoscale variation of the fiber radius and its iterative modification with sub-angstrom accuracy. The achieved fabrication precision is the result of sub-angstrom sensitivity of the fiber radius variation in response to the applied annealing power and repeatability of this variation. The demonstrated iterative method is applicable to the fabrication of a broad class of SNAP devices with sub-angstrom precision including uniform and nonuniform chains of coupled microresonators with predetermined spectral characteristics. Generally, this method allows the creation of photonic circuits with smaller microresonators, down to 10 μm in axial length [11]. We suggest that with the improved fabrication the demonstrated sub-angstrom precision can be achieved without iterations. In addition, an order-of-magnitude improvement in fabrication precision, i.e., below 0.1 Å, is feasible with smaller iteration powers and more accurate fabrication and characterization processes.

#178745 - $15.00 USD Received 25 Oct 2012; revised 17 Nov 2012; accepted 20 Nov 2012; published 29 Nov 2012